Wavelength Dependence of the Nonlinear Absorption of C_{60}− and C_{70}−Toluene Solutions

J. Barroso, A. Costela,* I. García-Moreno, and J. L. Saiz

Instituto de Química Física "Rocasolano", Consejo Superior de Investigaciones Científicas, Serrano 119, 28006 Madrid, Spain

Received: December 2, 1997; In Final Form: January 29, 1998

The nonlinear transmission properties of C_{60} and C_{70} in toluene solution in the ultraviolet and visible spectral regions have been studied using nanosecond laser pulses. Whereas at 308 and 534 nm both fullerenes behave as reverse saturable absorbers, at 337 nm their behavior changes to that of a saturable absorber. A five-level rate equation model was developed that reproduces adequately the dependence of transmittance with intensity at the different irradiation wavelengths and allows us to estimate the absorption cross sections of the first excited singlet state for each fullerene.

Introduction

Numerous investigations have been carried out to study various properties of fullerenes. In particular, the intensity-dependent transmission exhibited by these molecules in both liquid and solid solution has attracted much attention because of the possible applications of fullerenes as optical limiters.[1−8] Optical limiting occurs when the transmittance of a material decreases with increasing laser fluence. The observed optical limiting behavior of fullerenes has been attributted to reverse saturable absorption (RSA), which occurs when the absorption cross section of the excited state is greater than that of the ground state.

The studies on the optical limiting properties of fullerenes have been mainly performed in C_{60} solutions at 532 nm irradiation wavelength,[1,3−6] although some studies in C_{70} solutions[1,2] and at wavelengths in the spectral range 420−700 nm[2,7,8] have also been reported. By using a suitable theoretical model, the dynamics of the RSA process can be studied,[4,6] and from a comparison of the experimental data with theoretical curves, the excited-state absorption cross sections can be estimated.[2]

In this paper, we have extended the study of the transmission properties of both C_{60} and C_{70} in toluene solution to the ultraviolet region of the spectrum and have found that at some specific wavelengths in this spectral region both fullerenes no longer act as reverse saturable absorbers but behave as saturable absorbers, with the transmittance increasing with laser fluence. A five-level model incorporating excited-state absorption was used to fit the experimental data and extract values for the absorption cross sections of the first excited singlet state. Usually, the absorption cross sections of the excited states are obtained from differential absorption spectra of the corresponding fullerene species.[9−12] Both C_{60} and C_{70} are characterized by a rapid and efficient intersystem crossing that results in a lifetime of the first excited singlet state of around 1 ns.[9−11,13] As a consequence, the direct determination of the absorption cross sections of these excited states requires the use of techniques with temporal resolution in the subnanosecond range. Here, we present a method that allows us to estimate the absorption cross sections of the excited states in a relatively simple way by using lasers working in the nanosecond regime. The appropriateness of our experimental and theoretical approach was checked by performing experiments at 534 nm irradiation wavelength, so that the results could be compared with those previously reported in the literature with irradiation in the same spectral region.

Experimental Section

A schematic diagram of the experimental arrangement is shown in Figure 1. An excimer laser (MPB Model AQX-150) was used as the light source in the ultraviolet region. When filled with the appropriate Xe/HCl/He mixture, this laser works as XeCl laser and generates output pulses of ∼100 mJ at 308 nm, with a duration of approximately 15 ns (full width at half-maximum, fwhm). When this same laser is filled with the appropriate N_2/He mixture to work as a N_2 laser, it produces ∼7 ns (fwhm) pulses of ∼1.7 mJ at 337 nm. Both the 337 and 308 nm beams have rectangular cross section.

The light source in the visible was a Q-switched, frequency-doubled Nd:KGW laser (Monocrom Model STR-2+), which generates 534 nm pulses of ∼5.5 mJ, with a duration of approximately 6 ns (fwhm) and a circular beam cross section.

A rectangular or circular aperture (A) was used to select a uniform intensity portion of the ultraviolet and visible laser beams, respectively, which was then focused onto the 1 mm thick quartz cell containing the fullerene solution using fused silica spherical lens/lenses, L_1 and/or L_2. With the Nd:KGW and XeCl lasers, a single 25 cm focal length lens was used, placed at position L_1 or L_2, respectively. With the N_2 laser, a combination of two lenses was used, with focal lengths 50 cm (L_1) and 10 cm (L_2). The pulse intensity at the cell was varied by placing appropriate calibrated attenuators (AT_1) at the output of the lasers. A quartz beam splitter (B) positioned in the laser path before the cell with the C_{60}− or C_{70}−toluene solution, directed ≈10% of the beam energy onto either a photodiode (Nd:KGW beam) or a monochromator (XeCl and N_2 beams). In the first case, a $f = 5$ cm fused silica spherical lens (L_5) was used to focus the light from the beam splitter into an optical fiber (OF) coupled to photodiode PD (SGD 100A). In the second case, the ultraviolet light was imaged onto the input slit of a McPherson 2035 monochromator (M_1) with either the above referred lens L_1 (337 nm light) or a 50 cm focal length fused

* FAX: +341 5642431. E-mail: acostela@iqfr.csic.es.

S1089-5639(98)00367-3 CCC: $15.00
Published on Web 03/21/1998

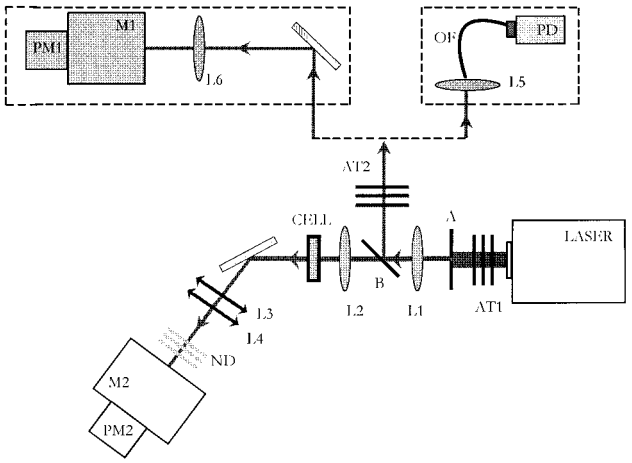

Figure 1. Schematic of experimental arrangement: A, aperture; AT, attenuators; B, beam splitter; L, lenses; M, monochromators; ND, neutral density filters; OF, optical fiber; PD, photodiode; PM, photomultiplier.

silica spherical lens (L_6, 308 nm beam) and detected with an EMI 9816 QB photomultiplier (PM_1). Calibrated attenuators (AT_2) were placed in the beam paths when appropriate.

The light transmitted by the cell with the C_{60}− or C_{70}−toluene solution was directed onto a second monochromator (M_2, Applied Photophysics M300) and detected with a RCA 1P28 photomultiplier (PM_2). With the ultraviolet beams, two crossed fused silica cylindrical lenses (L_3 and L_4), with positive (15 cm) and negative (−15 cm) focal lengths, respectively, placed in the transmitted beam path, optimize the detection by adapting the signal beam cross section to the input slit of monochromator M_2. Calibrated neutral density filters (ND) were used before monochromator M_2 to ensure linear operation of photomultiplier PM_2 over the whole range of transmitted intensities.

The photodiode PD and photomultiplier PM_1 responses were calibrated with respect to the energy incident in the cell as measured by pyroelectric energy meters (GenTec ED200 and ED100A). The response of photomultiplier PM_2 to the transmitted light was then calibrated with PD and PM_1. The calibration procedure was performed in two steps for each irradiation wavelength, with and without the empty cell placed in the path of the light beam, which allowed to correct the transmitted signal for reflection and absorption losses in the quartz cell. The signals from photodiode PD and photomultipliers PM_1 and PM_2 were averaged over 16 shots at 1 Hz repetition rate and displayed on digital oscilloscopes (Tektronix 468 and 2430A). The temporal characteristics of the different light beams were measured with a fast rise-time photodiode (ITL TF1850) and Tektronix 7934 storage oscilloscope incorporating a Tektronix DC501 CCD camera which allows us to digitize the analogue signals displayed on the oscilloscope screen.

The cross section of the light beams at the position of the cell was determined by placing thermal paper in that position. The area of the darkened region was measured using a ×100 microscope and utilized to calculate the light intensity incident in the cell. In the above-described experimental conditions, these areas were found to be 9×10^{-4}, 2.3×10^{-3}, and 7.2×10^{-2} cm^2 for the 534, 337, and 308 nm beams, respectively. No damage was detected in the quartz cell even at the highest intensities used.

Fullerenes were obtained by arc-vaporizing graphite under 350 mbar of helium in a reactor built following the directions of Scrivens and Tour.[14] Once the fullerene mixture is formed in the arc, it is extracted from the soot with toluene, placing

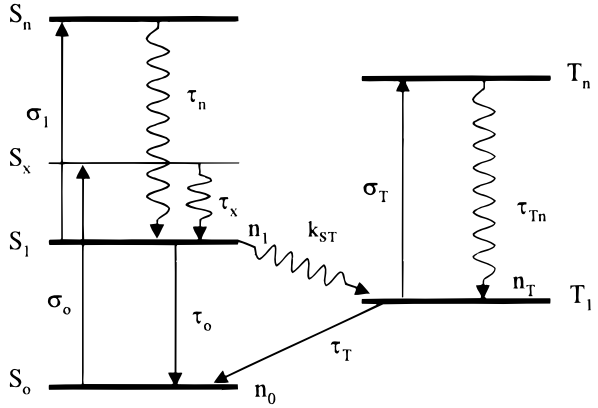

Figure 2. Energy level diagram.

the reactor in an ultrasonic bath. The nonsoluble material was separated from the extract by centrifugation at 6000 rpm and filtration in WCVP Millipore membranes with 0.1 μm pore size. The extract was then concentrated and dried using a roto-vap at ≈80 °C and 0.01 mbar.

Separation of C_{60} and C_{70} from the obtained product was accomplished by column liquid chromatography on PGH graphite powder according to a method based on that of Spitsyna et al.[15] C_{60} with 99.5% purity and C_{70} with 98% purity were obtained from the first and last fractions, respectively. The analysis was carried out by high-performance liquid chromatography (HPLC) in Kontron 325 HPLC chromatograph with a 432 detector and a 250 × 4 mm column filled with Spherisorb ODS2 (5 μm grain size), at a detector wavelength of 330 nm. The moving phase was toluene:acetonitrile 50:50.

The characteristics and purity of the products and solvents used are as follows: Graphite rods, 120 mm length and 6 mm diameter, from Le Carbone Lorraine, PT quality; carbon disulfide (BDH), spectroscopic grade; acetonitrile (Scharlau), HPLC grade, 99.85%; toluene (Romil Chemicals), HPLC grade, 99.9%. The solvents were used as received.

Solutions of C_{60} and C_{70} in toluene with concentrations in the range 10^{-4}−10^{-3} M, depending on the irradiation wavelength, were prepared. For C_{60}−toluene solutions, the concentration was chosen so that the transmission of the samples in our experimental conditions at the highest intensities used was ∼10%. For C_{70}, solutions with the same optical density as the C_{60} solutions at the different wavelengths were prepared.

Fullerene molecules in solution have been shown to degrade at high laser power densities by a photolysis mechanism, especially under irradiation of UV light.[16] To ascertain that sample degradation is not affecting the measurements, UV−visible absorption spectra of the C_{60}− and C_{70}−toluene solutions were taken before and after each experiment with a Cary 1E UV−visible spectrophotometer. The spectra before and after irradiation were phenomenologically identical. This invariance of the spectra excluded any appreciable effect of photodegradation in our experimental conditions. Nevertheless, to avoid any possible local effect caused by transient accumulation of degraded molecules in the irradiated region, each averaged measurement was taken after waiting for at least 1.5 min.

Theoretical Model

A five level model involving the ground state S_0, first excited S_1, and higher excited S_n singlet states, and lowest T_1 and higher T_n triplet states (Figure 2) has been used to compute the intensity-dependent transmittance of the C_{60}− and C_{70}−toluene solutions. Similar models have been used before in the study

of RSA in fullerene solutions.[2−4,6,7] The laser radiation excites molecules from the ground- state S_0 to a vibrational substate S_x of either the first electronic excited singlet-state S_1 or a higher-lying singlet state,[9,17] with an absorption cross section σ_0. The molecules in this state S_x decay rapidly (τ_x = picoseconds) to the equilibrium singlet-state S_1. This level relaxes either to the ground state, with rate $1/\tau_0$, or to the triplet-state T_1, with rapid intersystem crossing rate k_{ST}, of the order of 10^{-9} s^{-1} [9−11,13] (intersystem crossing yield $\phi_{ST} \approx 1$[11,18−20]). The intrinsic triplet relaxation time τ_T is very slow, on the order of tens (C_{60}) or hundreds (C_{70}) of microseconds,[9,11,18−21] although it is shortened to the range of hundreds of nanoseconds in air-saturated solution.[18,19] The molecules in S_1 and T_1 can be excited by subsequent absorption of laser radiation to higher singlet S_n and triplet T_n states, with absorption cross sections σ_1 and σ_T, respectively. These excited states decay rapidly (τ_n, τ_{T_n} less than picoseconds) back to S_1 and T_1 so that it can be assumed that states S_1 and T_1 are not depopulated by light absorption.

Taking into account the above considerations, the level system in Figure 2 can be described in good approximation, for irradiation with nanosecond pulses, by the following set of rate equations:

$$\frac{\partial n_0}{\partial t} = -\sigma_0 I n_0 + \frac{n_1}{\tau_0} + \frac{n_T}{\tau_T} \quad (1)$$

$$\frac{\partial n_1}{\partial t} = \sigma_0 I n_0 - \frac{n_1}{\tau_0} - n_1 k_{ST} \quad (2)$$

$$\frac{\partial n_T}{\partial t} = n_1 k_{ST} - \frac{n_T}{\tau_T} \quad (3)$$

$$\frac{\partial I}{\partial t} = \frac{c}{n_r}\frac{\partial I}{\partial z} = -\frac{cI}{n_r}[\sigma_0 n_0 + \sigma_1 n_1 + \sigma_T n_T] \quad (4)$$

In eqs 1−4 only the time variation of populations n_0, n_1, and n_T of energy levels S_0, S_1, and T_1, respectively, has been accounted for, as the populations of levels S_x, S_n, and T_n can be neglected because of the very short lifetimes of those levels. I represents the photon flux (photons cm^{-2} s^{-1}), c is the speed of light in a vacuum and n_r the solution refractive index (n_r = 1.46 for toluene at 25 °C). In the eq 4, $\partial I/\partial z$ describes the change of photon flux as the laser light propagates through the sample (z being the propagation direction). The radiative lifetime τ_0 of the first excited singlet state and the intersystem crossing rate constant k_{ST} relate to the lifetime τ of that state through the relationship

$$\frac{1}{\tau} = \frac{1}{\tau_0} + k_{ST} \quad (5)$$

The differential rate equations were solved numerically using a fourth-order Runge−Kutta routine[22] with the following boundary conditions

$$n_0(t=-\infty,z) = n = n_0 + n_1 + n_T \quad (6)$$

$$n_1(t=-\infty,z) = n_T(t=-\infty,z) = 0 \quad (7)$$

The shape of the incident laser pulse has been assumed to be Gaussian:

$$I(t,z=0) = I_0 \exp(-t^2/2\sigma_t^2) \quad (8)$$

where I_0 is the peak photon flux at $z = 0$ and σ_t is the root-mean-square (rms) width of the Gaussian function, related to the fwhm pulse duration t_p by $t_p = 1.1774\sigma_t$.

TABLE 1: Photophysical Parameters of C_{60} and C_{70} in Toluene Solution Used in the Numerical Computations

parameter[a]		value C_{60}	value C_{70}	ref
τ (ns)		1.3	0.7	13
$\phi_{ST} = k_{ST}\tau$		0.96	0.9	18,19
τ_T (ns)		>150	>190	estimated
$\sigma_0(\lambda)$ (cm^2)	λ = 308 nm	5.6×10^{-17}	8.2×10^{-17}	this work
	λ = 337 nm	1.5×10^{-16}	9.4×10^{-17}	this work
	λ = 534 nm	3.2×10^{-18}	2.1×10^{-17}	this work
$\sigma_T(\lambda)$ (cm^2)	λ = 308 nm	9.1×10^{-17}	9.8×10^{-17}	this work, 12
	λ = 337 nm	9.2×10^{-17}	9.4×10^{-17}	this work, 12
	λ = 534 nm	1.4×10^{-17}	4.2×10^{-17}	this work, 12

[a] τ, lifetime of first excited singlet state; ϕ_{ST}, intersystem crossing quantum yield; k_{ST}, intersystem crossing rate constant; τ_T, first triplet state relaxation time; σ_0, ground-state absorption cross section; σ_T, first triplet-state absorption cross section.

Results and Discussion

The equations of the model were solved with all the parameters appearing in them being kept constant except σ_1, which was considered as a free parameter and allowed to vary until the experimental data were reproduced. The values of the fixed photophysical parameters used in eqs 1−5 are collected in Table 1.

The lifetimes of the S_1 states of C_{60} and C_{70} are independent of solution concentration and excitation wavelength.[11,23] Their values in toluene solution are taken to be 1.3 ± 0.2 ns and 0.7 ± 0.05 ns, respectively, as determined by Lee et al.[13] in picosecond transient absorption studies. These values are in good agreement with those obtained by Ebessen et al.[9,10] (1.2 and 0.7 ns) and Palit et al.[11] (1.45 and 0.66 ns) by pico- and nanosecond laser-flash photolysis techniques and by Yang et al.[23] (1.2 and 0.6 ns) by time-resolved photoluminiscence measurements.

The quantum yield of the triplet formation has been consistently found to be unity or near unity[11,18−20] and independent of the excitation wavelength.[11,20] We have used in our model the values determined by Arbogast et al. for C_{60} at 532 nm[18] and for C_{70} at 355 nm.[19]

The lifetime and the nature of decay of the C_{60} and C_{70} triplet state T_1 are dependent on the pulse energy and concentration of ground state.[9−12] When deoxygenated solutions with fullerene concentrations on the order of or lower than 10^{-4} M are irradiated with low-energy pulses, values of 40−50 μs[11,18,20,21] and 90−300 μs[9,11,12,19] for the intrinsic triplet lifetimes of C_{60} and C_{70}, respectively, are obtained. These values decrease to 330 and 730 ns, respectively, in air-saturated solutions.[18,19] When higher concentrations and/or irradiation energies are used, both ground-state quenching and triplet−triplet annihilation processes increase their influence in the deactivation kinetics of triplet excited states T_1 of C_{60} and C_{70}.[9−12] Using the values determined by Dimitrijevic and Kamat[12] for the ground-state quenching (2×10^8 M^{-1} s^{-1} for $^3C_{60}$* and 6×10^8 M^{-1} s^{-1} for $^3C_{70}$*) and triplet−triplet annihilation (1.8×10^9 M^{-1} s^{-1} for $^3C_{60}$* and 2×10^9 M^{-1} s^{-1} for $^3C_{70}$*), and the values obtained by Arbogast et al.[18,19] for the quenching rate constant by oxygen (2×10^9 M^{-1} s^{-1} for $^3C_{60}$* and 9×10^8 M^{-1} s^{-1} for $^3C_{70}$*), the lower limits for τ_T quoted in Table 1 are estimated in our experimental conditions. As these relaxation times from the first triplet states of C_{60} and C_{70} are much longer than the laser pulse widths, the term n_T/τ_T in eqs 1 and 3 can be neglected.

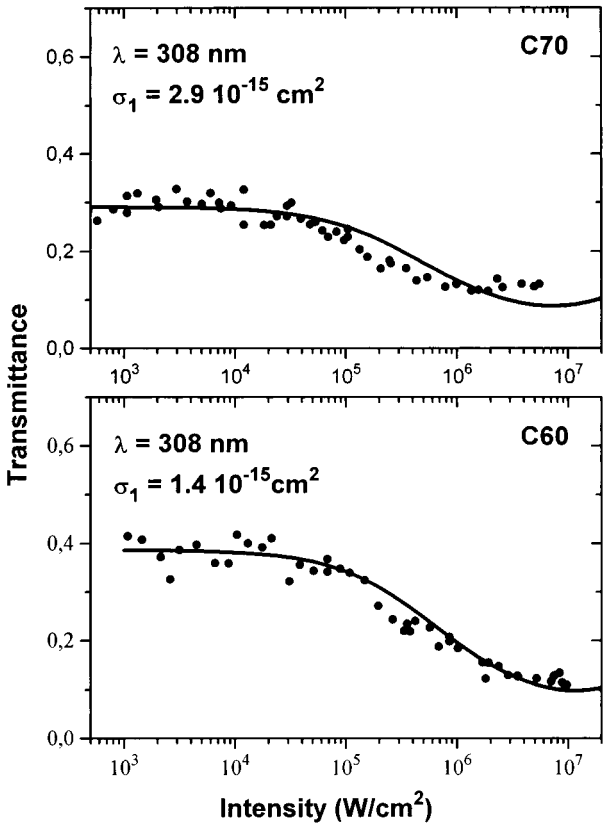

Figure 3. Transmittance as a function of intensity (full circles) of C_{60} and C_{70} in toluene solution for irradiation at 308 nm with pulses from a XeCl laser. The solid curves are the transmission predictions of the theoretical model obtained with the indicated values of σ_1.

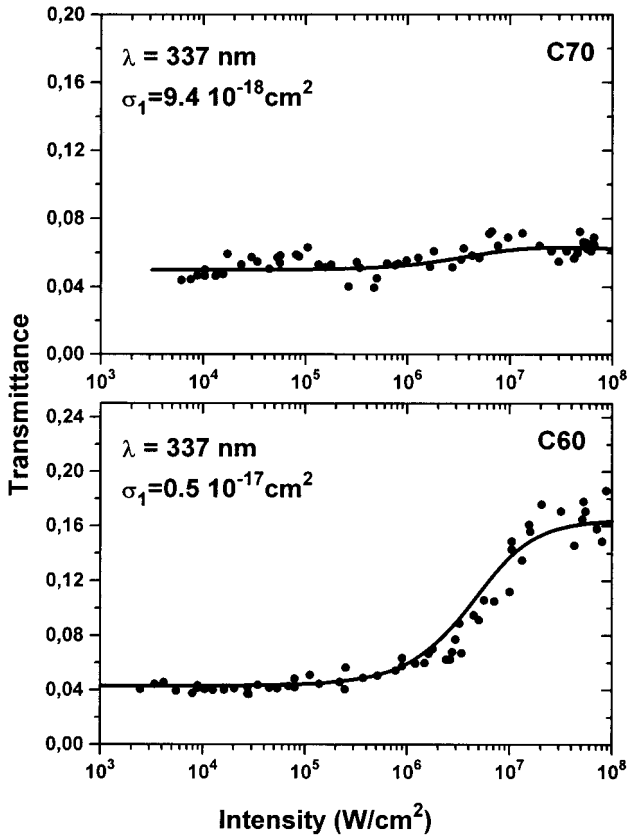

Figure 4. Transmittance as a function of intensity (full circles) of C_{60} and C_{70} in toluene solution for irradiation at 337 nm with pulses from a N_2 laser. The solid curves are the transmission predictions of the theoretical model obtained with the indicated values of σ_1.

Molar decadic extinction coefficients of the ground state ϵ_0 (M^{-1} cm^{-1}) at the different irradiation wavelengths were obtained from the C_{60} and C_{70} absorption spectra. The absorption cross sections σ_0 (Table 1) were determined from the extinction coefficients by using the relationship

$$\sigma_0 = 0.385 \times 10^{-20}\epsilon_0 \tag{9}$$

where σ_0 is given in cm^2.

The triplet state absorption cross sections σ_T reported in Table 1 were determined by combining the values of the extinction coefficients of the ground state obtained in this work with the difference extinction coefficients $\Delta\epsilon = \epsilon_T - \epsilon_0$ obtained from the time-resolved difference absorption spectra of $^3C_{60}$* and $^3C_{70}$* as reported by Dimitrijevic and Kamat.[12] In the case of irradiation at 534 nm, the values so obtained for C_{60} and C_{70} are 7% and 20% lower, respectively, than those reported in Table 1. As discussed below, this increase in the values of σ_T at 534 nm was necessary in order to properly reproduce the experimental data.

Experiments were performed where the intensity of the laser pulses incident onto the cell with the fullerene solutions was varied for up to 5 orders of magnitude. The transmitance data obtained for both C_{60}− and C_{70}−toluene solutions at the three irradiaton wavelengths (308, 337, and 534 nm) are shown in Figures 3−5. The particular concentrations used in each case are given in Table 2. In all cases, the highest incident fluence was kept lower than 1 J/cm^2, as it has been shown[4] that at higher fluences some nonlinear and higher-order processes, not included in the simple five-level model considered in this work, became relevant. The intensity incident on the samples was lowered in controlled steps until the small-signal transmission regime was reached, that is, until a constant transmittance, independent of intensity, was obtained. The small-signal transmittance (T) values so obtained are given in Table 2. After taking into account the losses in the quartz cell, these transmittance values are identical to those calculated from the small-signal expression:

$$T = \exp(-\alpha l) \tag{10}$$

where $\alpha = \sigma_0 n$ is the solution absorption coefficient and l is the thickness of the sample cell.

When correcting the transmitted signal for reflection and absorption losses in the quartz cell, as described in the Experimental Section, it was found that whereas at 534 and 337 nm the system behaves linearly (in the sense that the transmittance of the cell was constant over the range of intensities used), that is not so for irradiation at 308 nm. In this last case it was found that the transmittance of the empty cell depended on the incident intensity, probably due to residual absorption by the cell material. It was then necessary to obtain a calibration curve covering the whole range of intensities used before performing any actual experiment. The curve of calibration was the same independent of the cell being empty or filled with toluene.

The solid lines in Figures 3−5 represent the results of the model calculations, obtained with the appropriate values of the photophysical parameters (Table 1) and with σ_1 as a free parameter. When previously discussing how the values of σ_T reported in Table 1 were obtained, we indicated that the procedure we followed produced values of σ_T at 534 nm somewhat lower than those reported in Table 1. With the values first obtained ($\sigma_T(534) = 1.3 \times 10^{-17}$ and 3.4×10^{-17} cm^2 for

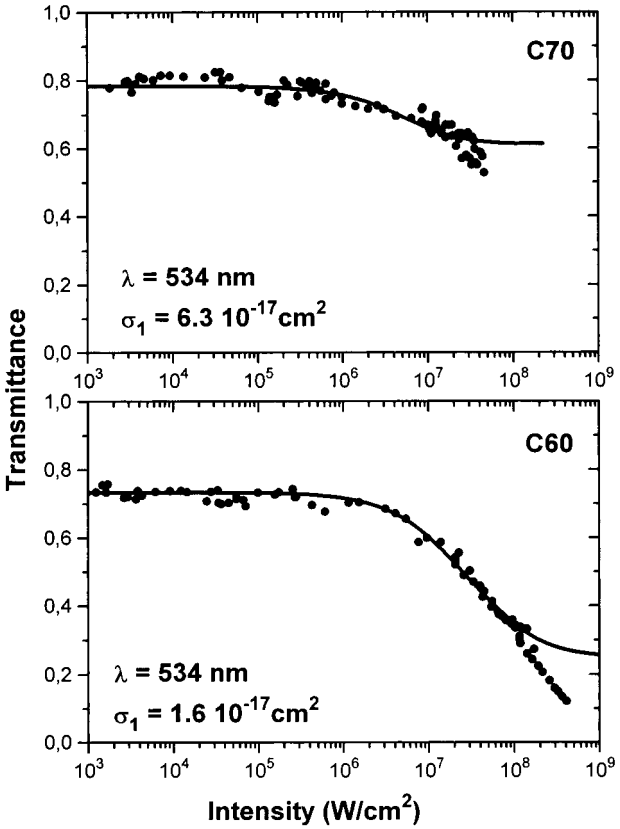

Figure 5. Transmittance as a function of intensity (full circles) of C_{60} and C_{70} in toluene solution for irradiation at 534 nm with pulses from a Nd:KGW laser. The solid curves are the transmission predictions of the theoretical model obtained with the indicated values of σ_1.

TABLE 2: Concentrations (*C*) of C_{60} and C_{70} in Toluene Solution Used at the Different Irradiation Wavelengths and Small-Signal Transmittance (*T*) through the 1-mm Path-Length Sample Cell

irradiation wavelength (nm)	$C \times 10^3$ (M)		T	
	C_{60}	C_{70}	C_{60}	C_{70}
308	0.28	0.25	0.39	0.29
337	0.36	0.54	0.04	0.05
534	1.67	0.19	0.73	0.78

C_{60} and C_{70}, respectively) we were unable to fit the whole set of data in Figure 5 with any value of σ_1. From the triplet−triplet absorption spectra of C_{60} and C_{70} in benzene solution reported by Bensasson et al.,[24,25] the values $\sigma_T(534) = 1.7 \times 10^{-17}$ and 3.8×10^{-17} cm^2 for C_{60} and C_{70}, respectively, can be obtained. These values are higher than our initial estimations; thus, we proceeded to increase the values of σ_T we had obtained in steps of 0.1×10^{-17} cm^2, until the experimental data could be reasonably fitted with an appropriate value of σ_1. For C_{60}−toluene, the value $\sigma_T(534) = 1.4 \times 10^{-17}$ cm^2 produced the solid curve in Figure 5a when $\sigma_1(534) = 1.6 \times 10^{-17}$ cm^2. This value of σ_1 at 534 nm is the same that can be obtained from the experimental data of Ebessen et al.,[10] which supports the appropriateness of the approach here used. As explained above, the theoretical model is expected to fail at high fluences. Such a failure is apparent in the lack of reproducibility of the 534 nm C_{60}−toluene experimental data at intensities higher than 10^8 W/cm^2.

The values of σ_1 that best fitted the experimental data are indicated in each plot and collected in Table 3. In the plots corresponding to the C_{60}−toluene solutions, changes of σ_1 greater than 20−40% (depending on the irradiation wavelength)

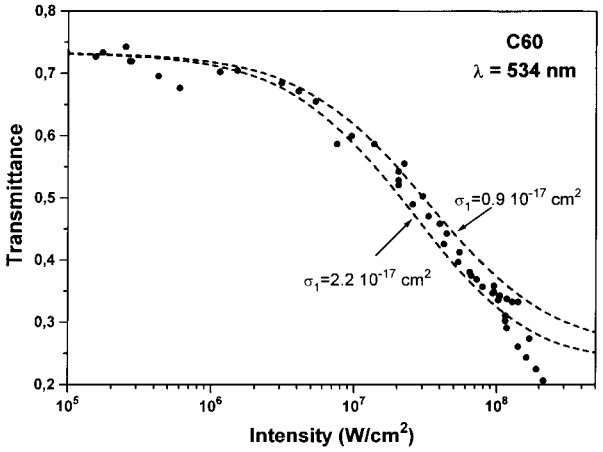

Figure 6. Effect on the model predictions of varying the value of σ_1. The experimental data (full circles) correspond to C_{60}−toluene solution irradiated at 534 nm.

TABLE 3: Model Predictions of Adjustable Parameter σ_1 (Absorption Cross Section of the First Excited Singlet State) at the Different Irradiation Wavelengths

irradiation wavelength (nm)	σ_1 (cm^2)	
	C_{60}	C_{70}
308	1.4×10^{-15}	2.9×10^{-15}
337	0.5×10^{-17}	9.4×10^{-18}
534	1.6×10^{-17}	6.3×10^{-17}

result in significant deviations of the theoretical curves from the experimental behavior. As an example, in Figure 6 is presented the effect on the theoretical curves of changing the value of σ_1 by 40%, with respect to the best fitting value, in the 534 nm case. It can be considered that the two curves in Figure 6 define a region of admissible values of σ_1. Thus, the width of this region can be considered as a measure of the predicting capabilities of the theoretical model here used. In the C_{70}−toluene solutions, the sensitivity of the fitting to the value of σ_1 is similar at the 308 and 534 nm irradiation wavelengths. With irradiation at 337 nm, the change of transmittance with intensity for the C_{70}−toluene solution was very small (Figure 4) and as a result a wider range of values of σ_1 produced reasonable fits to the experimental data, with variations of up to 75% in the value of σ_1 reported in Table 3 being admitted by the model.

It is inmediately apparent from the data presented in Figure 3−5 the different behavior of the fullerene solutions depending on the irradiation wavelength: they behave as reverse saturable absorbers at 534 and 308 nm but as saturable absorbers at 337 nm. These differences in behavior can be easily understood when the relative values of σ_1, σ_T, and σ_0 (Tables 1 and 3) are taken into account. It is well-known that RSA occurs when the absorption cross section from excited-state electronic energy levels is higher than the ground-state absorption cross section. In the present case, in both C_{60} and C_{70} solutions the singlet and triplet excited-state absorption cross sections, σ_1 and σ_T, are greater than the ground-state absorption cross section, σ_0, at both 534 and 308 nm irradiation wavelengths, whereas at 337 nm σ_T is somewhat lower than (C_{60}) or equal to (C_{70}) σ_0, and σ_1 is lower than σ_0 by at least 1 order of magnitude. Thus, only at 534 and 308 nm conditions are met for RSA to occur. At 534 nm the values of σ_1 and σ_T are nearly equal so that levels S_1 and T_1 should contribute similarly to RSA. On the contrary, at 308 nm σ_1 is much greater than σ_T and the main contribution to RSA should proceed from S_1.

From the experimental data of Ebessen et al.[10] and Tanigaki et al.,[9] the values 1.6×10^{-17} and 4.5×10^{-17} cm^2 can be obtained for the absorption cross sections of the first excited singlet state of C_{60} and C_{70}, respectively, at 534 nm irradiation wavelength. As can be seen from Table 3, the values predicted by the model here used for σ_1 at 534 nm are in good agreement with the experimental ones: for C_{60}, the theoretical value is equal to the experimental-based one, as noted above; for C_{70}, the value predicted by the model differs by 30% from that based on experiment, but this difference is within the margin of error allowed by the model, as discussed above. Henari et al.[2] have used a rate equation model to calculate ground- and excited-state absorption cross sections for C_{60} and C_{70} in benzene at a number of wavelengths between 440 and 610 nm. The values these authors obtained for the excited-state absorption cross sections of C_{60} and C_{70} at 520 nm are 2 and more than 1 order of magnitude higher, respectively, than those reported in Table 3 for irradiation at 534 nm. Likewise, the values they calculated for the ground-state absorption cross sections at 520 nm are $\sim$160 and $\sim$25 times higher than those determined experimentally in this work for C_{60} and C_{70}, respectively, at 534 nm (Table 1). The differences in absorption at 520 and 534 nm are not important enough[9,10] to explain the discrepancy. Rather it could be due to Henari et al. using in their model the value of 600 ps for the radiative lifetime of the first excited singlet state, whereas from the data in Table 1 and eq 5 this radiative lifetime is found to be 32.5 ns for C_{60} and 7 ns for C_{70}, respectively.

Summary and Conclusions

The nonlinear transmission properties of C_{60} and C_{70} in toluene solution in the ultraviolet and visible spectral regions have been studied. Irradiation of the samples was performed with nanosecond laser pulses at 308, 337, and 534 nm wavelength. The fullerene solutions exhibit reverse saturable absorption behavior at 308 and 534 nm but behave as saturable absorbers at 337 nm, with the onset of the nonlinear absorption ocurring at $\sim 10^5$ W/cm^2 at 308 nm and at $\sim 10^6$ W/cm^2 at 337 and 534 nm. A five-level theoretical model was used to compute the intensity-dependent transmittance of the C_{60} and C_{70} solutions. In the model, the absorption cross section σ_1 of the first excited singlet state was considered as a free parameter and allowed to vary until the experimental data were reproduced. In this way estimations of σ_1 could be obtained. The values obtained for σ_1 at 534 nm are in good agreement with those determined from previous experimental data reported by Ebessen et al.,[9,10] demonstrating the usefulness of the approach here used to estimate excited-state absorption cross sections.

Acknowledgment. This research was supported by Project MAT97-0705-C02-01 of the Spanish Comisión Interministerial de Ciencia y Tecnología.

References and Notes

(1) Tutt, L. A.; Kost, A. *Nature* **1992**, *356*, 225.
(2) Henari, F.; Callaghan, J.; Stiel, H.; Blau, W.; Cardin, D. J. *Chem. Phys. Lett.* **1992**, *199*, 144.
(3) Kost, A.; Tutt, L.; Klein, M. B.; Dougherty, T. K.; Elias, W. E. *Opt. Lett.* **1993**, *18*, 334.
(4) McLean, D. G.; Sutherland, R. L.; Brant, M. C.; Brandelik, D. M.; Fleitz, P. A.; Pottenger, T. *Opt. Lett.* **1993**, *18*, 858.
(5) Justus, B. L.; Kafafi, Z. H.; Huston, A. L. *Opt. Lett.* **1993**, *18*, 1603.
(6) Li, C.; Zhang, L.; Wang, R.; Song, Y.; Wang, Y. *J. Opt. Soc. Am. B* **1994**, *11*, 1356.
(7) Couris, S.; Koudoumas, E.; Ruth, A. A.; Leach, S. *J. Phys. B: At. Mol. Opt. Phys.* **1995**, *28*, 4537.
(8) Smilowitz, L.; McBranch, D.; Klimov, V.; Robinson, J. M.; Koskelo, A.; Grigorova, M.; Mattes, B. R.; Wang, H.; Wudl, F. *Opt. Lett.* **1996**, *21*, 922.
(9) Tanigaki, K.; Ebessen, T. W.; Kuroshima, S. *Chem. Phys. Lett.* **1991**, *185*, 189.
(10) Ebessen, T. W.; Tanigaki, K.; Kuroshima, S. *Chem. Phys. Lett.* **1991**, *181*, 501.
(11) Palit, D. K.; Sapre, A. V.; Mittal, J. P.; Rao, C. N. R. *Chem. Phys. Lett.* **1992**, *195*, 1.
(12) Dimitrijevic, N. M.; Kamat, P. V. *J. Phys. Chem.* **1992**, *96*, 4811.
(13) Lee, M.; Song, O. K.; Seo, J. C.; Kim, D.; Suh, Y. D.; Jin, S. M.; Kim, S. K. *Chem. Phys. Lett.* **1992**, *196*, 325.
(14) Scrivens, W. A.; Tour, J. M. *J. Org. Chem.* **1992**, *57*, 6932.
(15) Spitsyna, N. G.; Buravov, L. I.; Lobach, A. S. *J. Anal. Chem.* **1995**, *50*, 613.
(16) Juha, L.; Hamplová, V.; Kubát, P.; Koudoumas, E.; Couris, S. *Chem. Phys. Lett.* **1994**, *231*, 314.
(17) Leach, S.; Vervloet, M.; Desprès, A.; Bréheret, E.; Hare, J. P.; Dennis, T. J.; Kroto, H. W.; Taylor, R.; Walton, D. R. M. *Chem. Phys.* **1992**, *160*, 451.
(18) Arbogast, J. W.; Darmanyan, A. P.; Foote, C. S.; Rubin, Y.; Diederich, F. N.; Alvarez, M. M.; Anz, S. J.; Whetten, R. L. *J. Phys. Chem.* **1991**, *95*, 11.
(19) Arbogast, J. W.; Foote, C. S. *J. Am. Chem. Soc.* **1991**, *113*, 8886.
(20) Terazima, M.; Hirota, N.; Shinohara, H.; Saito, Y. *J. Phys. Chem.* **1991**, *95*, 9080.
(21) Kajii, Y.; Nahagawa T.; Suzuki, S.; Achiba, Y.; Obi, K.; Shibuya, K. *Chem. Phys. Lett.* **1991**, *181*, 100.
(22) Press, W. H.; Flannery, B. P.; Teukolsky, S. A.; Vetterling, W. T. *Numerical Recipes, The Art of Scientific Computing*; Cambridge University Press: Cambridge, 1988; pp 550−560.
(23) Yang, L.; Dorsinville, R. *Opt. Commun.* **1996**, *124*, 45.
(24) Bensasson, R. V.; Hill, T.; Lambert, C.; Land, E. J.; Leach, S.; Truscott, T. G. *Chem. Phys. Lett.* **1993**, *201*, 326.
(25) Bensasson, R. V.; Hill, T.; Lambert, C.; Land, E. J.; Leach, S.; Truscott, T. G. *Chem. Phys. Lett.* **1993**, *206*, 197.